High sensitivity of simulated fog properties to parameterized aerosol activation in case studies from ParisFog

Pratapaditya Ghosh[1,2], Ian Boutle[3], Paul Field[3,4], Adrian Hill[3,5], Anthony Jones[3], Marie Mazoyer[6], Katherine J Evans[7], Salil Mahajan[7], Hyun-Gyu Kang[7], Min Xu[7], Wei Zhang[7], Noah Asch[1,2], and Hamish Gordon[8,2]

[1]Department of Civil and Environmental Engineering, Carnegie Mellon University, 5000 Forbes Avenue, Pittsburgh, 15213, United States
[2]Center for Atmospheric Particle Studies, Carnegie Mellon University, 5000 Forbes Avenue, Pittsburgh, 15213, United States
[3]Met Office, Fitzroy Road, Exeter, EX1 3PB, United Kingdom
[4]School of Earth and Environment, University of Leeds, Leeds, LS2 9JT, United Kingdom
[5]European Center for Medium-Range Weather Forecasting, Reading, UK
[6]CNRM, Université de Toulouse, Météo-France, CNRS, Toulouse, France
[7]Oak Ridge National Laboratory, Oak Ridge, TN, 37831, USA
[8]Department of Chemical Engineering, Carnegie Mellon University, 5000 Forbes Avenue, Pittsburgh, 15213, United States
Correspondence: gordon@cmu.edu

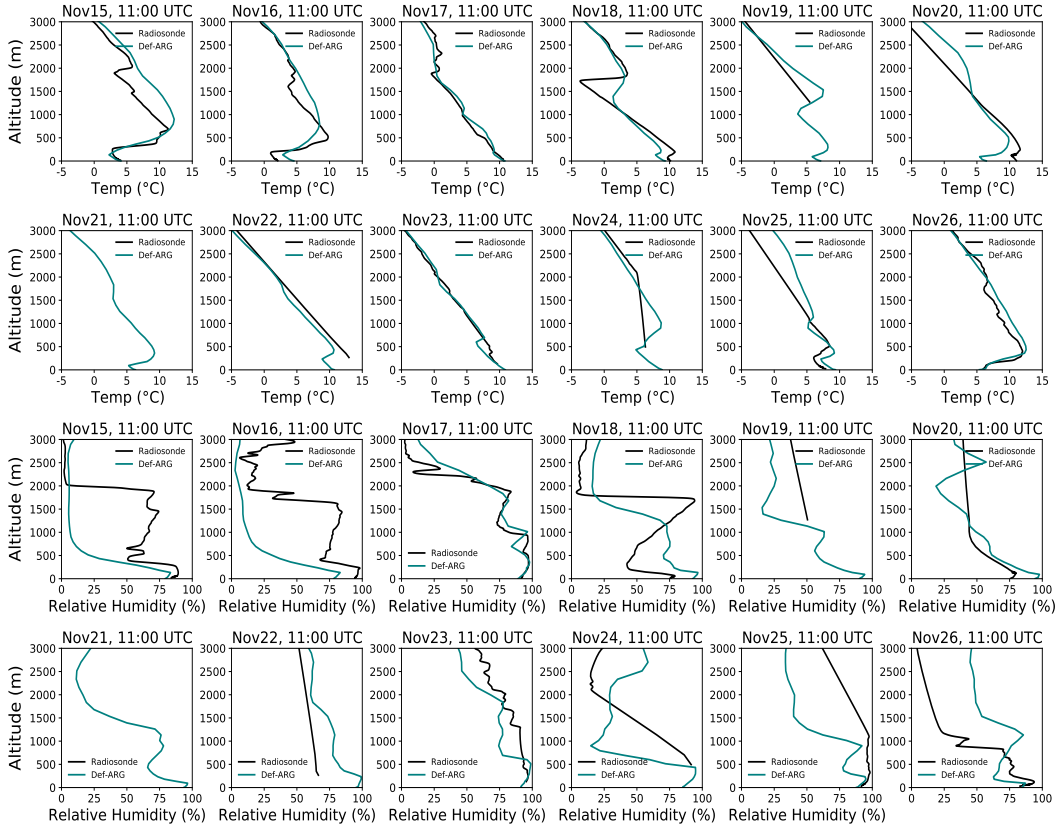

Figure S1: Temperature and relative humidity vertical profiles from our 500 m grid resolution Def-ARG simulation at 11:00 UTC each day, compared with the radiosonde data.

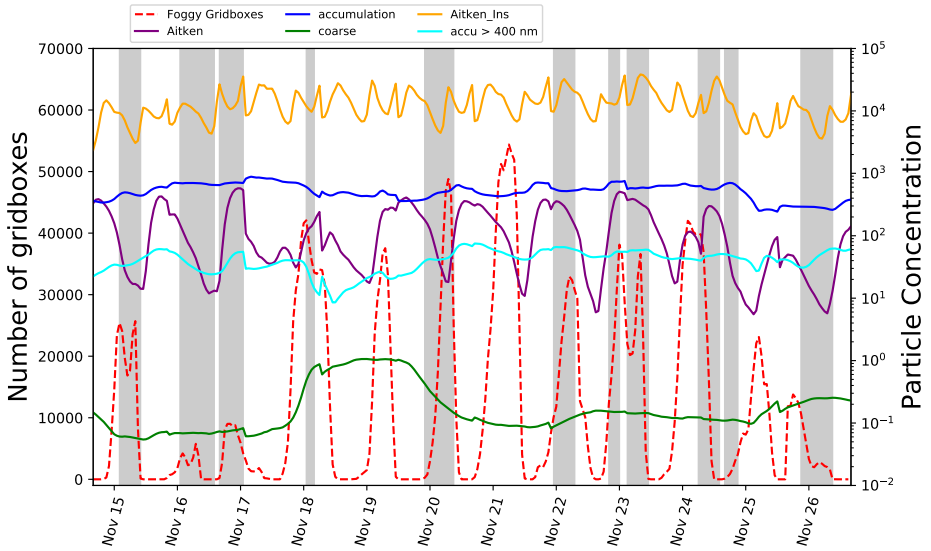

Figure S2: Timeseries of number of foggy gridboxes (Left Y axis) and particle number concentrations (Right Y axis) in the 500 m-resolution Def-ARG simulation. We demonstrate the domain mean number concentration of Aitken (soluble and insoluble), accumulation (total and > 400 nm diameter), and coarse mode aerosols simulated in the model at 5 m altitude.

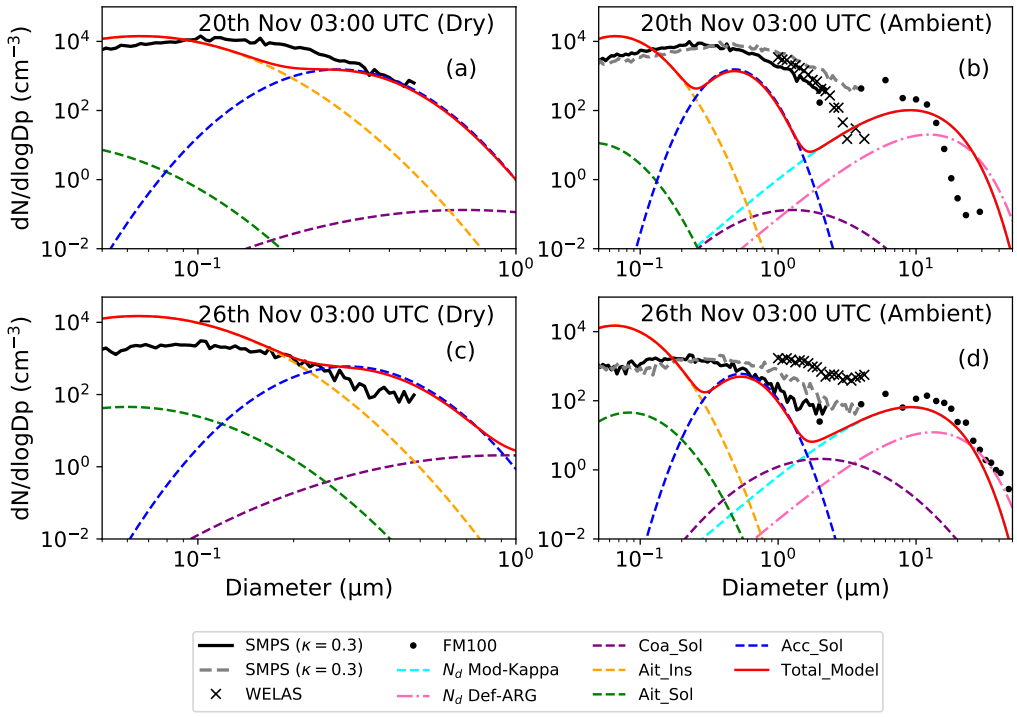

Figure S3: Dry and ambient aerosol size distribution on 20$^{\text{th}}$ (Top) and 26$^{\text{th}}$ (Bottom) November at 07:00 UTC from observations and the Mod-Kappa simulation. Only foggy grid cells are shown. The dry size distribution is measured by the SMPS only, while the WELAS and fog monitor (FM) observed the size distribution at ambient relative humidity. For this ambient size distribution, we also converted dry particle concentration data from the SMPS to ambient using κ-Köhler theory assuming a kappa value of 0.1 (and 0.3) and 100% relative humidity. The red line shows simulated total dry and ambient-humidity particle size distributions, while the dashed lines show the different aerosol and droplet modes. The model does not remove aerosols when they activate, so we subtract the N_d from the sum of the accumulation and coarse mode number concentration when plotting the red total number concentration curve to avoid double counting, but we leave the individual modes unchanged (so the red curve is slightly below the blue curve in the figure on 15 November. We also show the droplet size distribution from the Def-ARG simulation.

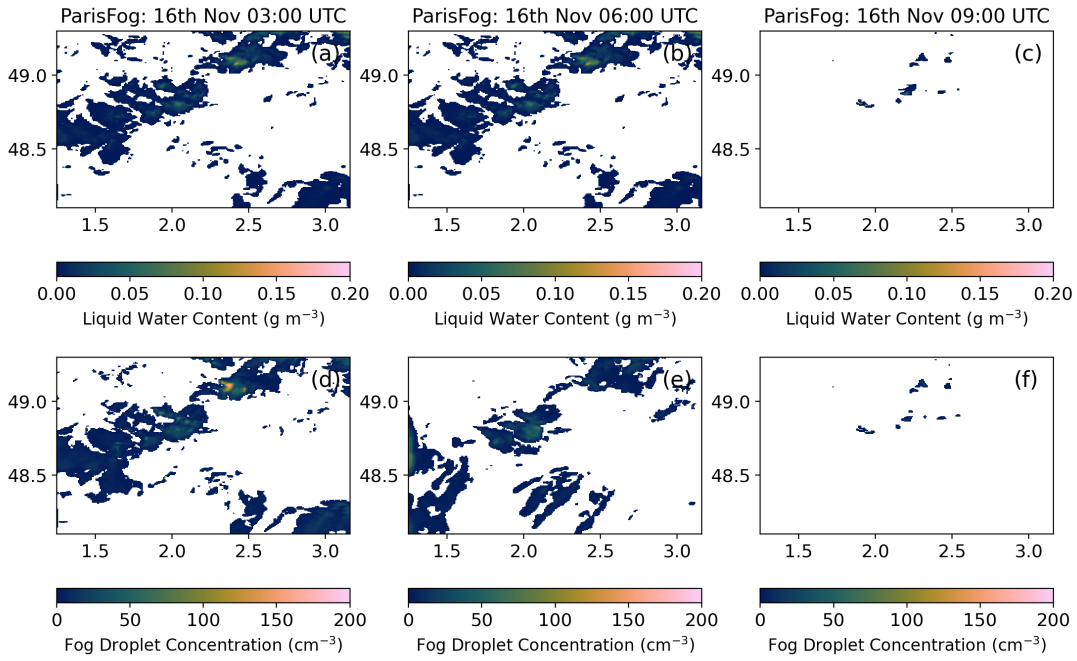

Figure S4: Spatial distribution of grid-mean liquid water content (top panel) and fog droplet number concentrations (bottom panel) at different times on 16$^{\text{th}}$ Nov from the 500 m resolution Def-ARG simulation at 5 m altitude.

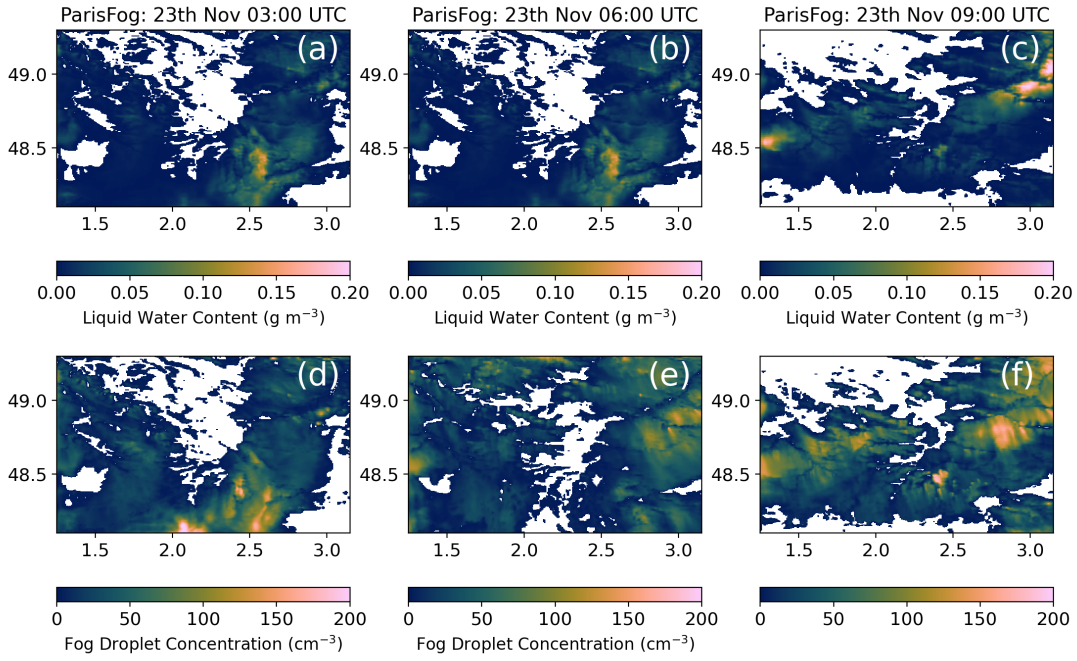

Figure S6: Spatial distribution of grid-mean liquid water content (top panel) and fog droplet number concentrations (bottom panel) at different times on 23$^{\text{th}}$ Nov from the 500 m resolution Def-ARG simulation at 5 m altitude.

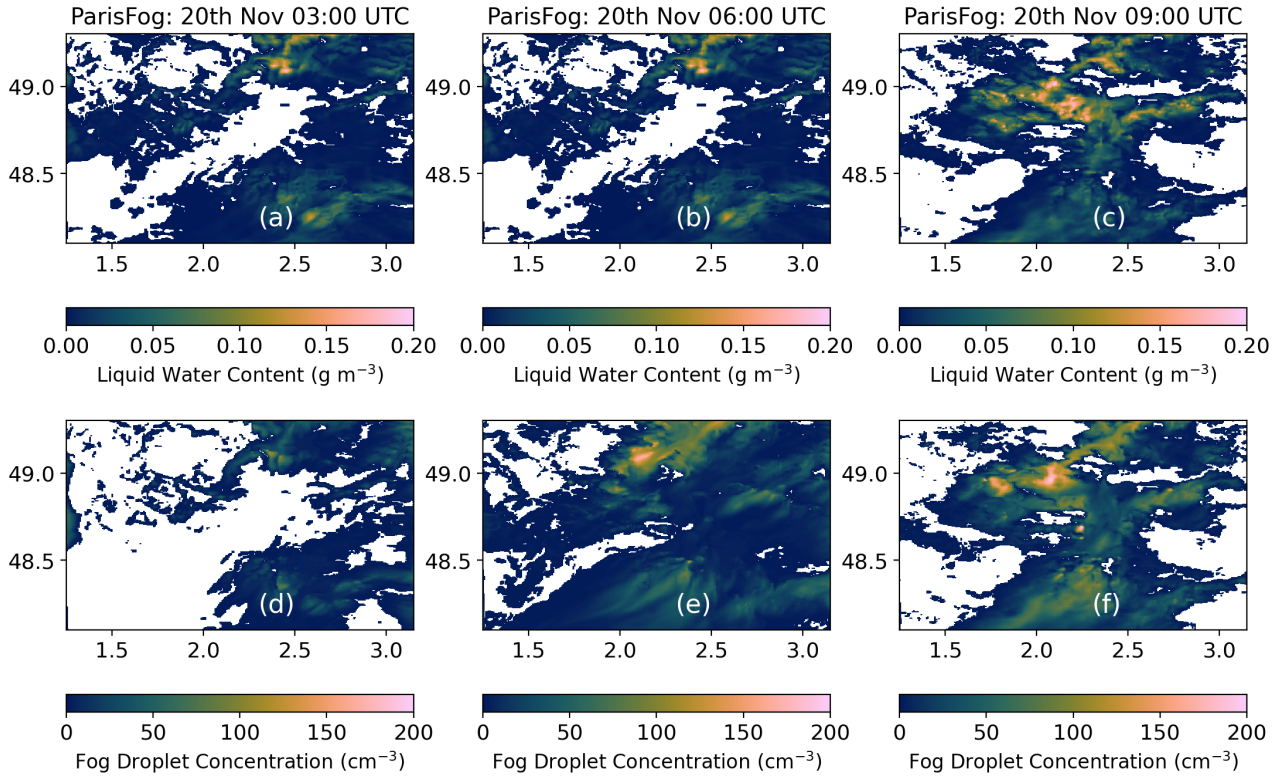

Figure S5: Spatial distribution of grid-mean liquid water content (top panel) and fog droplet number concentrations (bottom panel) at different times on 20$^{\text{th}}$ Nov from the 500 m resolution Def-ARG simulation at 5 m altitude.

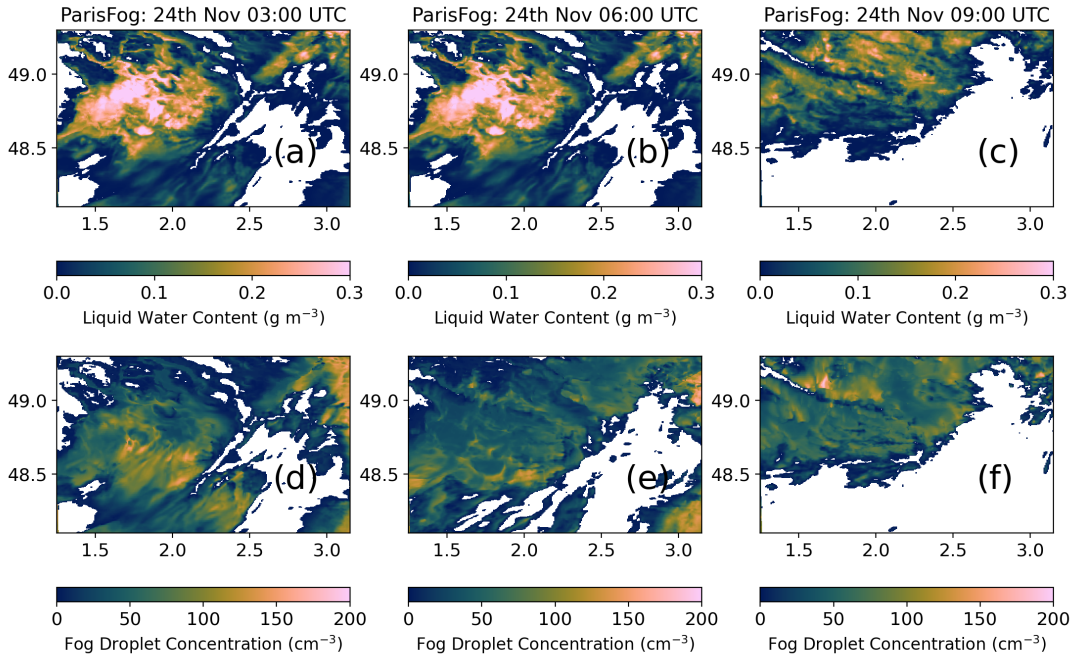

Figure S7: Spatial distribution of grid-mean liquid water content (top panel) and fog droplet number concentrations (bottom panel) at different times on 26$^{\text{th}}$ Nov from the 500 m resolution Def-ARG simulation at 5 m altitude.

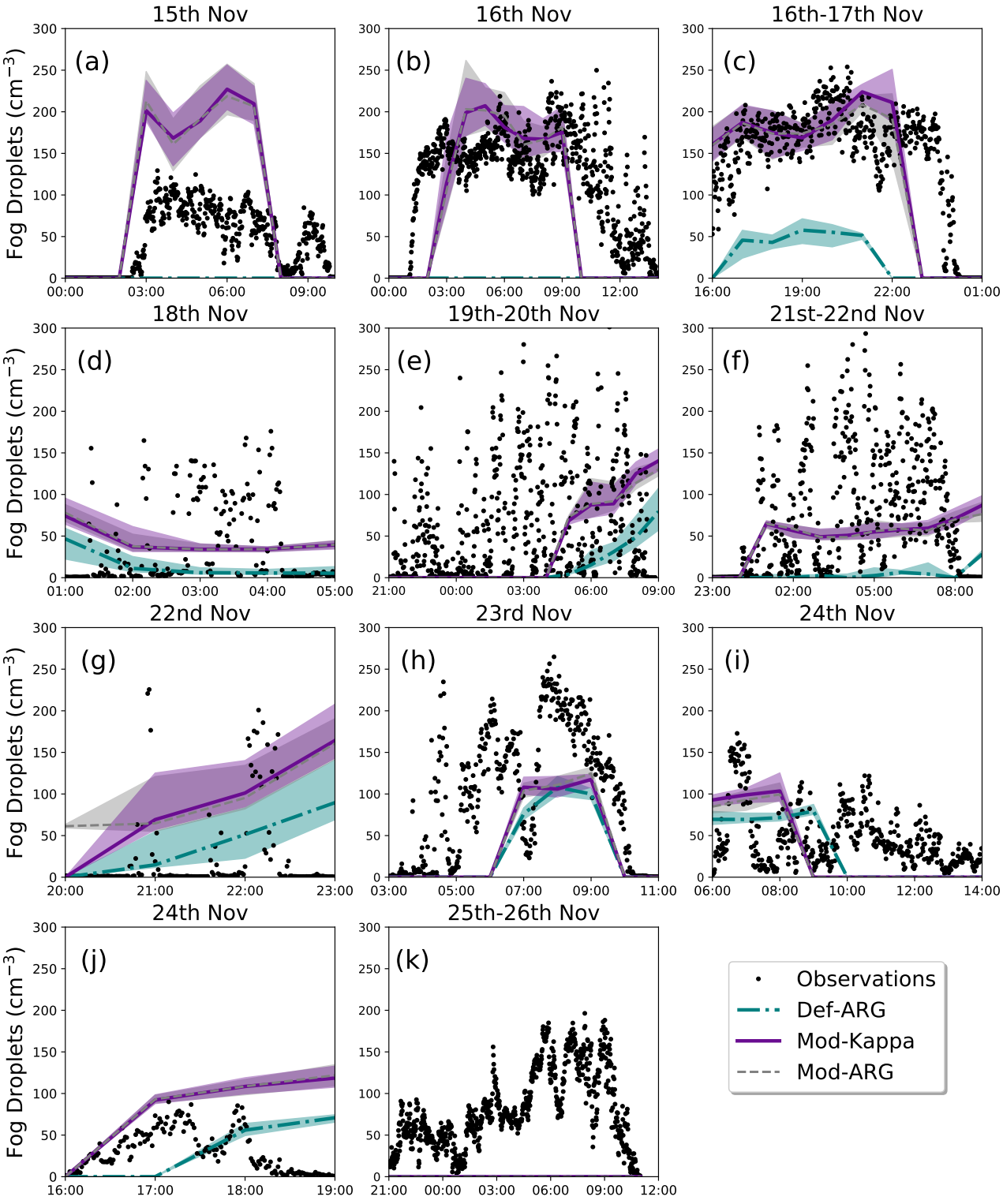

Figure S8: Variation of N_d as a function of time (UTC) for different fog events in the 500 m resolution regional simulations. Here we have used 20 × 20 boxes gridboxes around SIRTA to calculate median and interquartile ranges. Subplots (a-k) compare all the simulations with the observations for the different fog cases. The solid (and dashed) lines and shaded regions represent the median and interquartile range from foggy gridboxes.

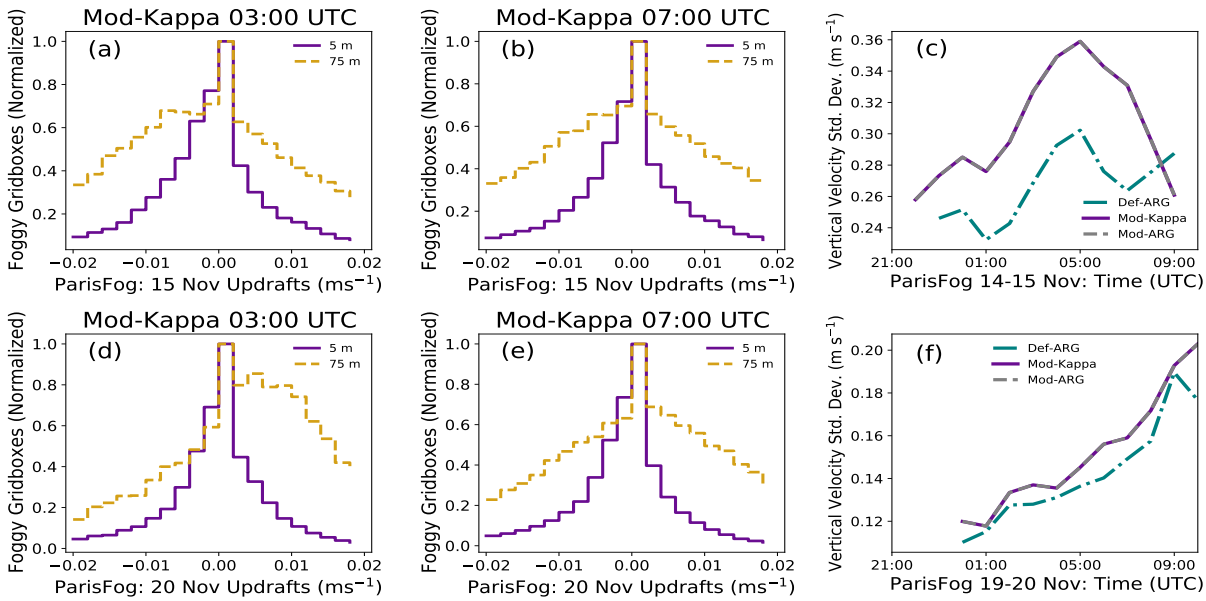

Figure S9: Histogram of updrafts at 5 m and 75 m altitude for two ParisFog cases at (a,d) 03:00 and (b,e) 07:00 UTC from the Mod-Kappa simulation. These panels show resolved updraft speeds, while the right panels (c,f) show the simulated standard deviation (σ_w) of sub-grid updrafts (the square root of the diagnosed subgrid updraft variance) from Def-ARG, Mod-ARG and Mod-Kappa simulations for the same fog cases at the surface. These results are from foggy gridboxes only.

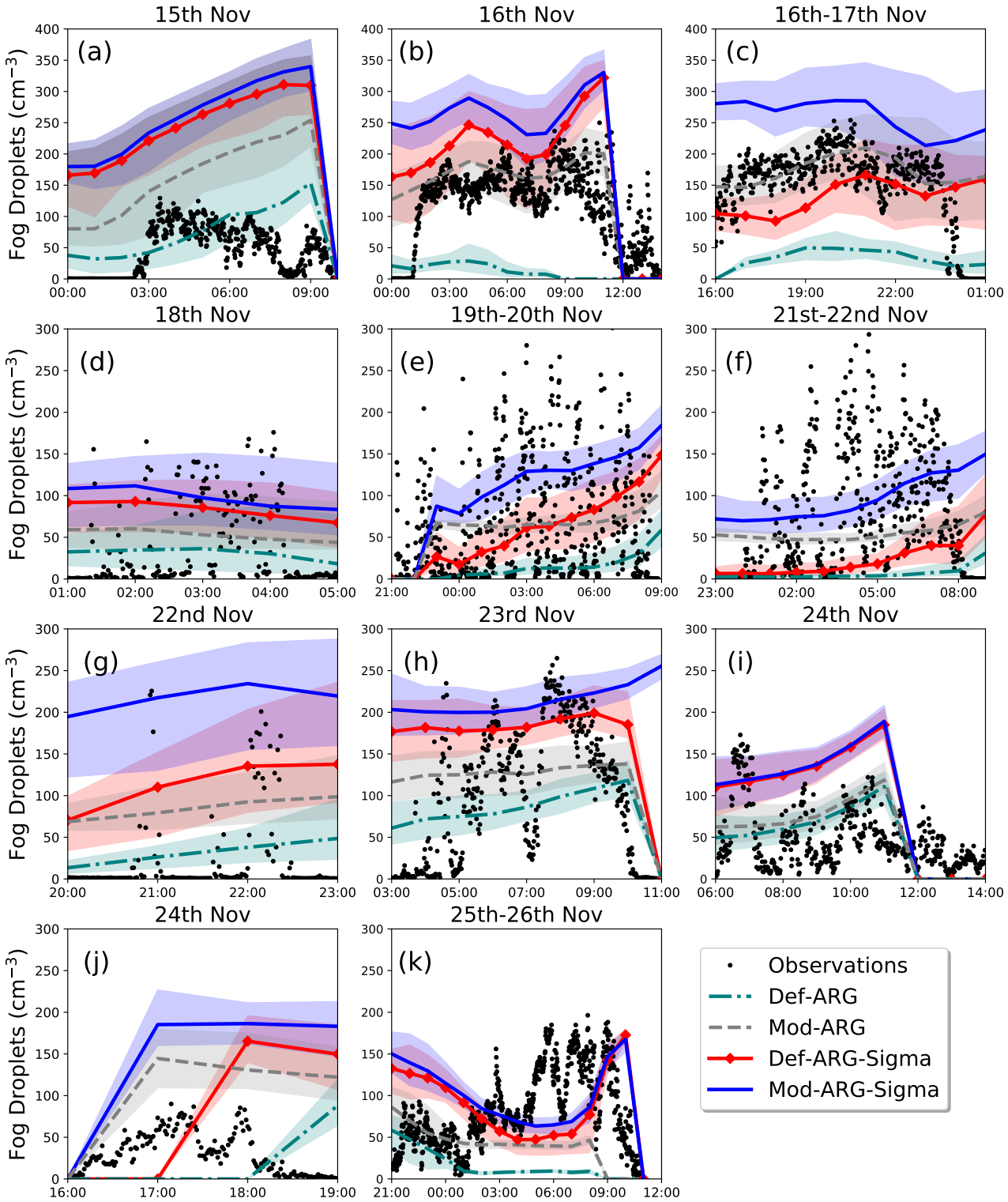

Figure S10: Variation of N_d as a function of time (UTC) for all the fog events in the 500 m resolution regional simulations, compared to observations from the fog monitor. We show results from Def-ARG, Mod-ARG, and corresponding simulations (Def-ARG-Sigma and Mod-ARG-Sigma), in which a sub-grid component is introduced to the updraft speed used in the aerosol activation scheme. In simulations Def-ARG-Sigma and Mod-ARG-Sigma, the updraft for activation is $w_{act} = w + c\,\sigma_{wsub}$, where σ_{wsub} is the width of updraft distribution (the square root of the diagnosed sub-grid vertical velocity variance), and the prefactor c is set to 0.2. w_{act} and w are the activation updraft and resolved (grid-scale) updraft respectively. In Supplement Figure S1 of the companion paper, we show that σ_{wsub} at the surface is overestimated by a factor of 5 for the LANFEX fog case we study (for which we have a turbulent kinetic energy dataset). However, for these ParisFog cases the prefactor is not motivated by model evaluation (we believe the simulated σ_{wsub} is closer to observations of vertical velocity variance), and so the prefactor is an ad-hoc tuning. The solid (and dashed) lines and shaded regions represent the median and interquartile range from foggy gridboxes.

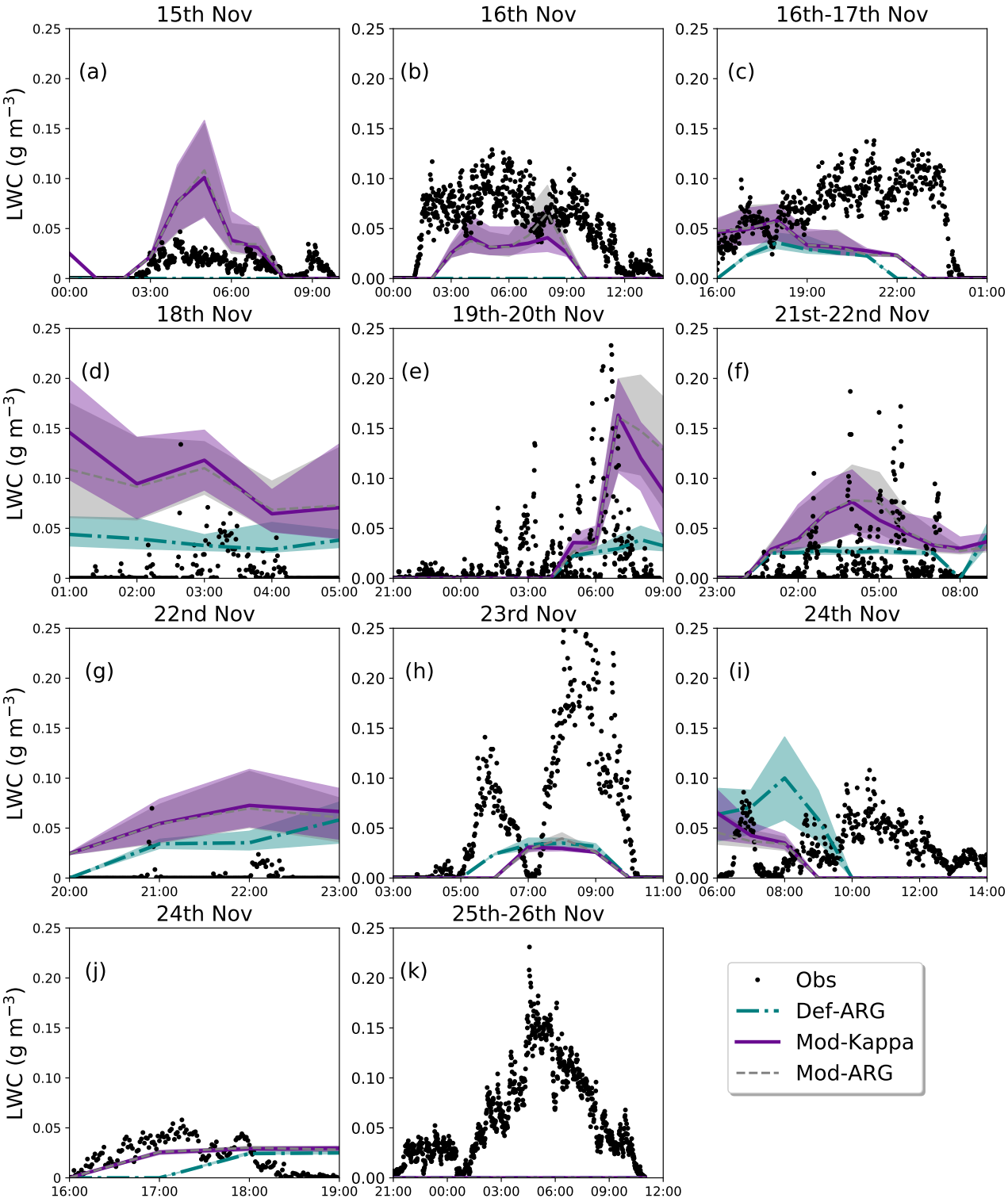

Figure S11: Variation of LWC as a function of time (UTC) is shown here for different fog events in the 500 m resolution regional model. Here we have used 20 × 20 boxes gridboxes around SIRTA to calculate median and interquartile ranges. Subplots (a-k) compare all the simulations with the observations for the different fog cases. The solid (and dashed) lines and shaded regions represent the median and interquartile range from foggy gridboxes.

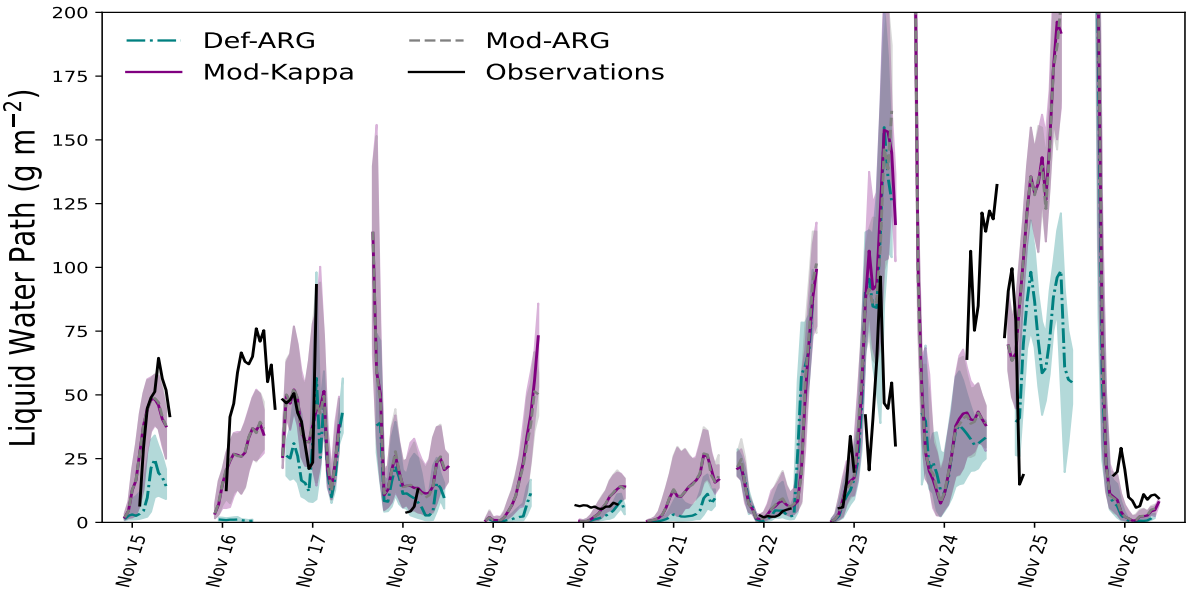

Figure S12: Time series of Liquid Water Path during the parisFog cases with and without radiative cooling included in aerosol activation for simulations Def-ARG, AD and AD-RAD.

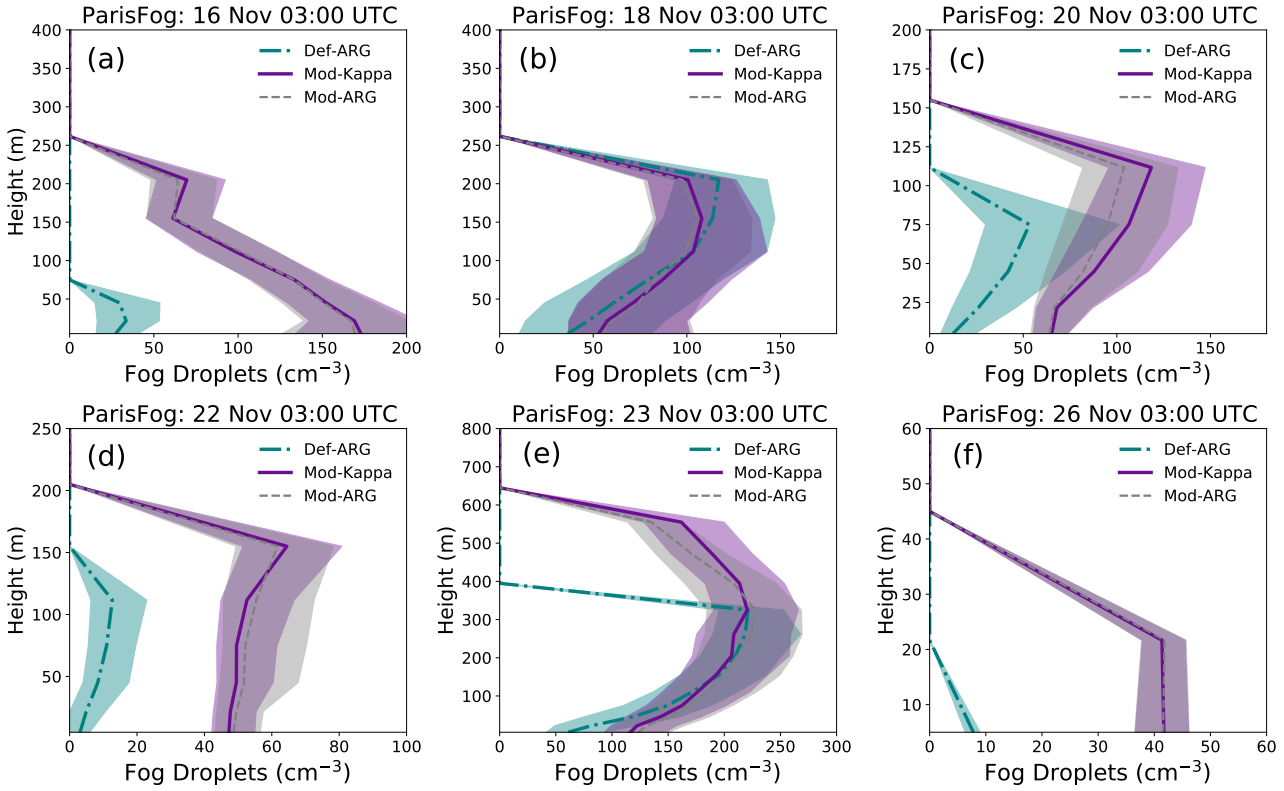

Figure S13: Variation of simulated droplet N_d in the 500 m-resolution model as a function of height for different fog events. Note the different y axis limits between subfigures. The solid and dashed lines represent the median values, and the shaded regions represent the interquartile ranges over foggy gridboxes. The solid and dashed lines represent the median values, and the shaded regions represent the interquartile ranges over the foggy gridboxes. We have picked columns that are entirely foggy till our threshold of 1000 gidboxes.

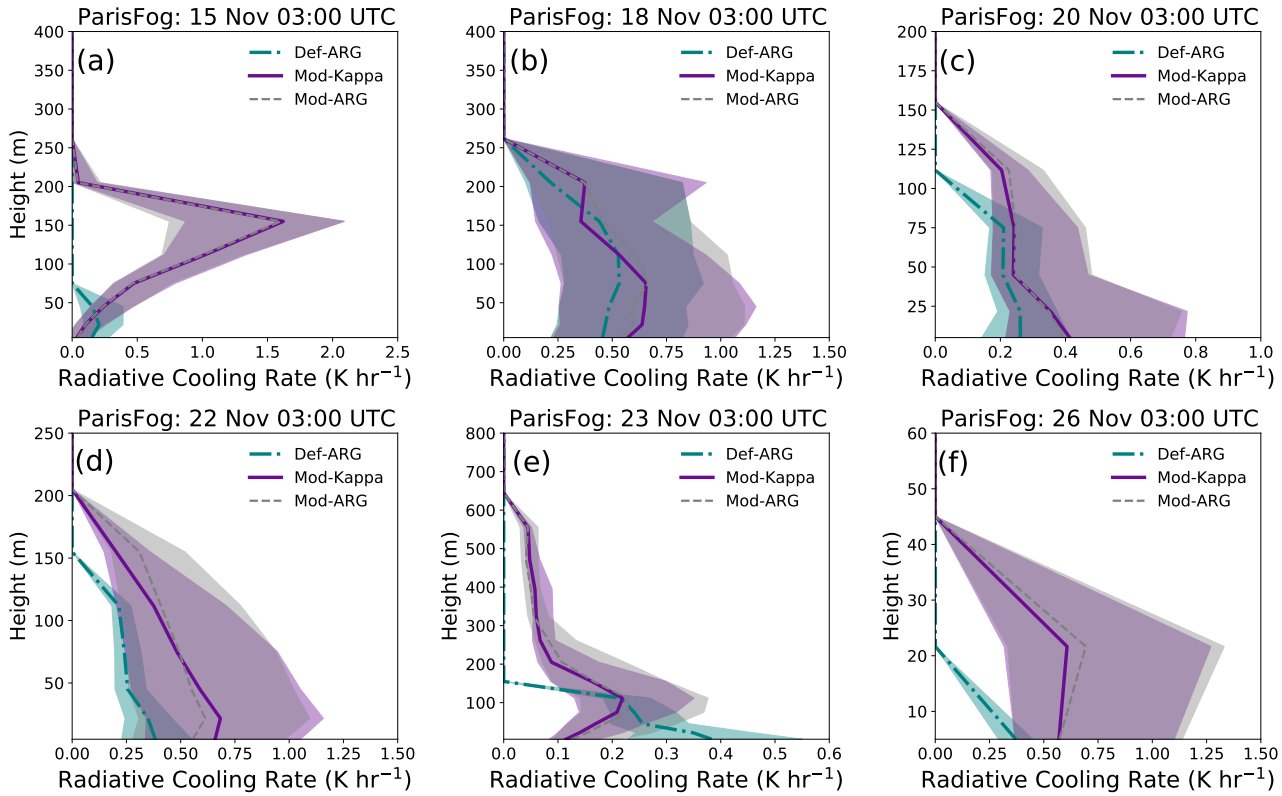

Figure S14: Variation of simulated radiative cooling rates in the 500 m-resolution model as a function of height for different fog events. Note the different y axis limits between subfigures. The solid and dashed lines represent the median values, and the shaded regions represent the interquartile ranges over foggy gridboxes. The solid and dashed lines represent the median values, and the shaded regions represent the interquartile ranges over the foggy gridboxes. We have picked columns that are entirely foggy till our threshold of 1000 gidboxes.

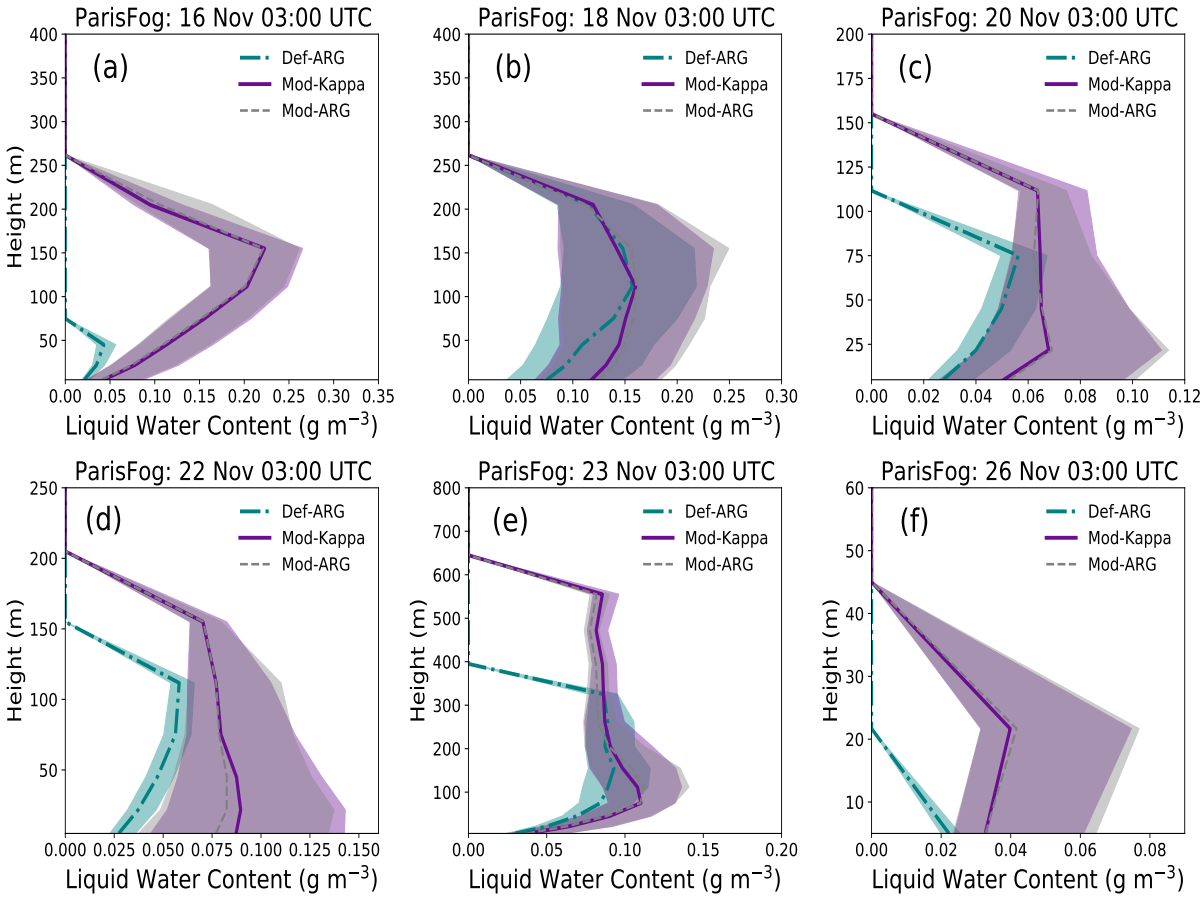

Figure S15: Variation of simulated LWC in the 500 m-resolution model as a function of height for different fog events. Note the different y axis limits between subfigures. The solid and dashed lines represent the median values, and the shaded regions represent the interquartile ranges over foggy gridboxes. The solid and dashed lines represent the median values, and the shaded regions represent the interquartile ranges over the foggy gridboxes. We have picked columns that are entirely foggy till our threshold of 1000 gidboxes.

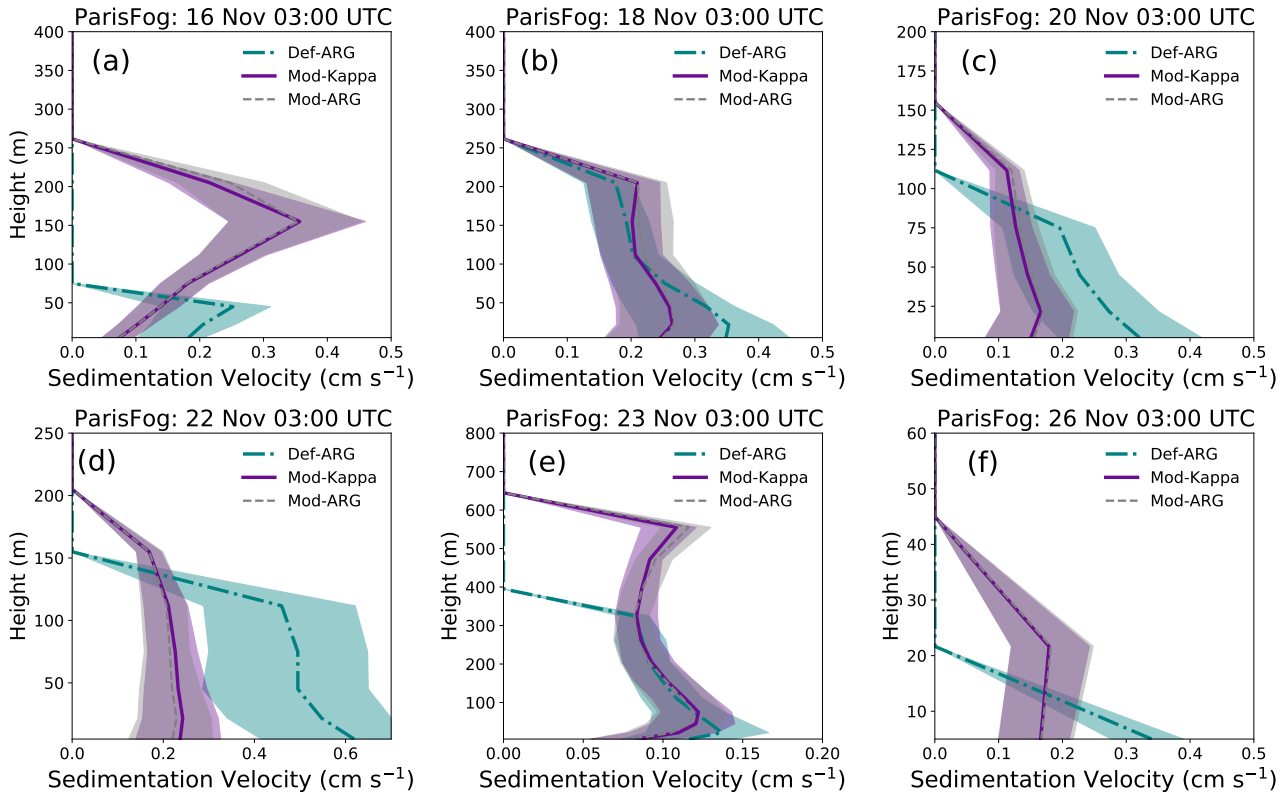

Figure S16: Variation of simulated droplet sedimentation velocity in the 500 m-resolution model as a function of height for different fog events. Note the different y axis limits between subfigures. The solid and dashed lines represent the median values, and the shaded regions represent the interquartile ranges over foggy gridboxes. The solid and dashed lines represent the median values, and the shaded regions represent the interquartile ranges over the foggy gridboxes. We have picked columns that are entirely foggy till our threshold of 1000 gidboxes.

Table S1: Normalized Mean Bias Factor (NMBF) for N_d for different simulations (500 m model) for all fog cases.

Fog Case	**Def-ARG**	**Mod-ARG**	**Mod-Kappa**
Nov 15 02:30	0.72	2.71	2.71
Nov 16 01:10	-8.96	0.23	0.22
Nov 16 16:00	-3.32	0.24	0.24
Nov 18 01:30	0.01	0.76	0.82
Nov 19 22:00	-5.20	-0.42	-0.42
Nov 21 23:50	-8.76	-0.18	-0.20
Nov 22 20:50	0.54	3.15	3.23
Nov 23 03:25	-0.15	0.29	0.50
Nov 24 06:20	0.07	0.21	0.23
Nov 24 16:10	-0.06	3.24	3.16
Nov 25 21:40	-3.84	-0.92	-0.67

Table S2: Normalized Mean Error Factor (NMEF) for N_d across different simulations (500 m model) for all fog cases.

Fog Case	**Def-ARG**	**Mod-ARG**	**Mod-Kappa**
Nov 15 02:30	0.99	2.76	2.76
Nov 16 01:10	9.21	0.37	0.36
Nov 16 16:00	3.46	0.31	0.30
Nov 18 01:30	0.72	1.01	1.03
Nov 19 22:00	5.86	1.01	1.01
Nov 21 23:50	9.65	0.85	0.84
Nov 22 20:50	0.85	3.15	3.23
Nov 23 03:25	0.60	0.58	0.82
Nov 24 06:20	0.72	0.80	0.81
Nov 24 16:10	2.02	3.42	3.34
Nov 25 21:40	4.20	0.97	0.84